

# Optoelectronic Properties and Memories Based on Organic Single-Crystal Thin Films

CHONG-YANG LIU AND ALLEN J. BARD\*

*Department of Chemistry and Biochemistry,  
The University of Texas at Austin, Austin, Texas 78712*

Received April 8, 1998

Organic and organometallic materials are promising candidates for molecular electronic devices. In addition to the currently commercialized liquid crystal displays, there are light-emitting diodes and other displays, transistors, memories, and photoelectric devices on the horizon.<sup>1–10</sup> Interest in organic materials for these applications arises from the huge number of structures available in this class of compounds and the possibility of tuning electrical and optical properties over a wide region by purposeful design. Encouragement for these views comes from the fact that conductivities in organic materials (crystals, polymers) vary by over more than 20 orders of magnitude (from TTF-TCNQ to Teflon) and that complex biological systems utilize organics. Before such devices can be realized, however, a better understanding of the structural factors that control the electrical and optical properties of organic solids is needed. These include studies of the nature of charge carriers and the factors that control their mobility. Especially important are the effects of traps (crystal defects, grain boundaries, impurities) on the electrical properties. The nature of contacts to the organic devices and the factors that control charge transfer at the metal contact/organic crystal interface are also of importance in device fabrication. In this Account we deal with single-crystal thin films and their electric and spectroscopic properties and discuss their potential application in memory devices for reversible, high-density optoelectronic data storage.

In contrast to inorganic solids, molecules in organic molecular crystals (OMCs) are generally widely spaced apart and held together by rather weak van der Waals forces (intermolecular energies  $\sim$  tenths of an electron-volt), which are at least an order of magnitude smaller than the intramolecular bond energies (2–4 eV). Conse-

quently, the inherent properties of the individual molecules are retained in the OMC to a large extent, e.g., as shown by the strong similarity between the optical spectra of OMCs and those of their constituent molecules.<sup>11–13</sup> This characteristic of OMCs, sometimes considered as oriented molecular gases, offers interesting opportunities to explore their potential for molecular electronics, since the unique properties of isolated molecules can be a useful guide to macroscopic properties when the molecules are arranged in the molecular crystal. For example, as discussed below, the orientational dependence of light absorption, detectable only with difficulty for polymer-supported solvent green 3 molecules, can be seen as sharply different colors with the naked eye in the single crystal.<sup>14</sup> The weak and long-distance intermolecular interactions cause only a slight perturbation in the electronic orbitals of the individual molecules in most OMCs, leading to a strong tendency for excitons and charge carriers to be localized on individual molecules<sup>11–13,15,16</sup> as compared to the complete delocalization in the bands of inorganic semiconductors with strongly bound atomic or ionic lattices, like Si and GaAs. As a result, charge carrier mobilities in OMCs are relatively low (typically  $<1 \text{ cm}^2 \text{ s}^{-1} \text{ V}^{-1}$ ) at room temperature and the carrier mean free path is essentially equal to the lattice constant because of strong scattering.<sup>11–13</sup> Indeed most OMCs are excellent electrical insulators, which makes them very useful, as discussed below, as memory media using charge trapping for data storage. The injected charges in these crystals can be held in a small ( $\sim$ nanometer scale) space for a long time. Moreover, many OMCs have high optical absorption coefficients ( $\alpha \approx 10^5$ ), and their electrical properties can be modulated significantly by irradiation over a rather wide spectral range, thus offering good possibilities for optical and optoelectronic devices.

To understand the electrical properties of OMCs, it is important to be able to model the way in which charges, electrons ( $e^-$ ) and holes ( $h^+$ ), move through the crystal. Charge transport in OMCs cannot be predicted quantitatively by current models. Band theory, which is well established for treating conductivity in inorganic solids, only describes motion of delocalized charges. In OMCs, although the  $\pi$ -electrons are delocalized and mobile within individual molecules, e.g., along conjugated chains of carbon atoms, injected excess charge cannot move easily from one molecule to another in the crystal, because of poor overlap in the wave functions of neighboring molecules. Thus, a hopping model is often employed, in which the charge moves between molecules by surmounting an energy barrier. This model accounts for many features of charge transport in OMCs but is still far from complete.<sup>11–13,15,16</sup>

An understanding of the properties of organic solids benefits from the experimental use of thin, single-crystal films rather than the polycrystalline or amorphous materials that often result from vacuum deposition or spin-

Chong-yang Liu was born in Shaanxi, China, and educated at Northwestern University, the Dalian Institute of Chemical Physics, the Chinese Academy of Sciences, and the Hahn-Meitner-Institut für Kernforschung Berlin, Germany, where he carried out research with Chen Yixuan, Li Wenzhao, Wang Hongli, and H. Tributsch, respectively. He was a Postdoctoral Fellow with Allen J. Bard and is presently a Research Scientist Associate at the University of Texas at Austin.

Allen J. Bard holds the Hackerman-Welch Regents' Chair in Chemistry at the University of Texas at Austin. His principle research interests are in the application of electrochemical techniques to the study of chemical problems.

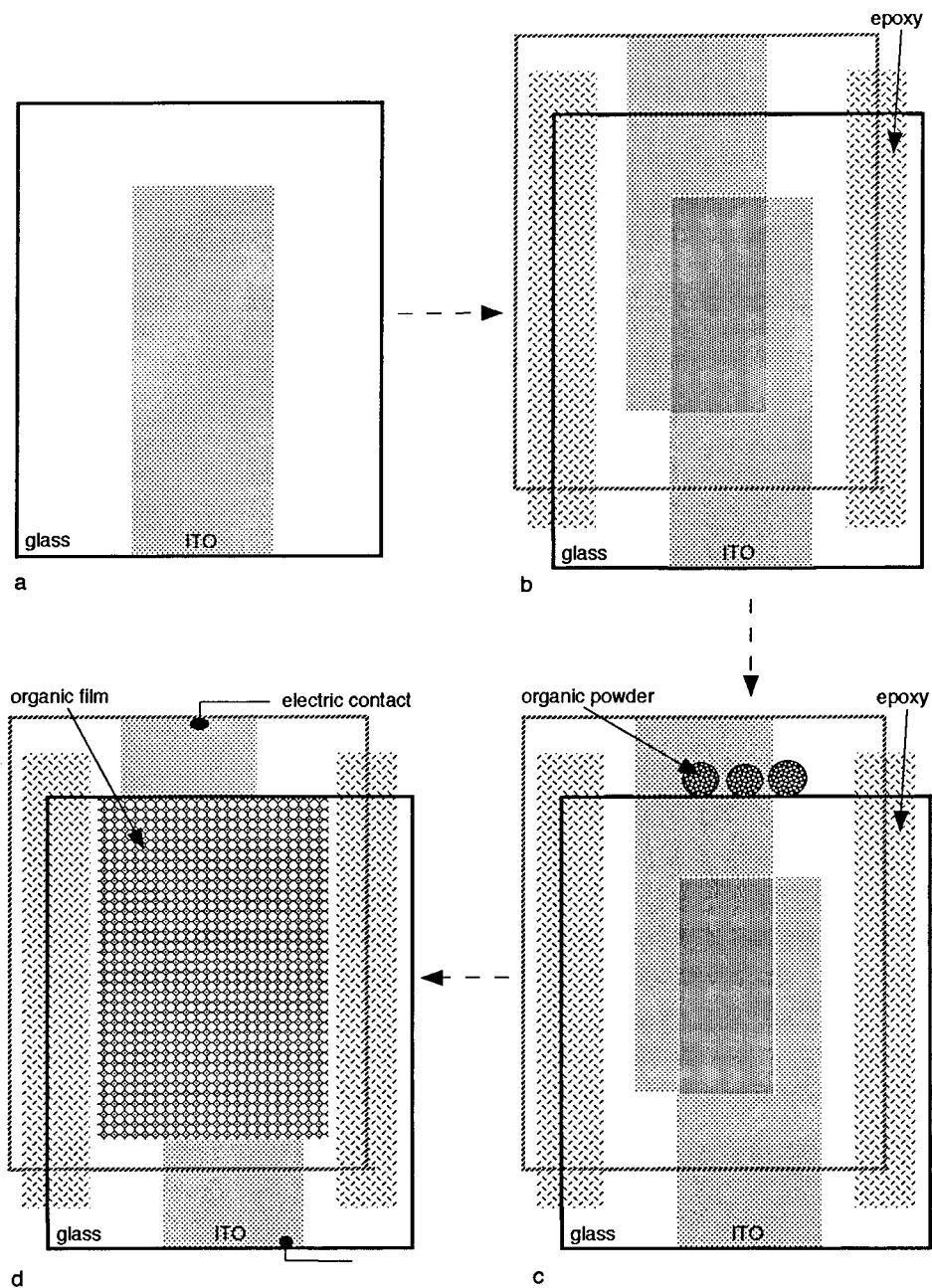


**FIGURE 1.** Schematic diagram of cell fabrication. (a) ITO removed on three sides. (b) Epoxy cement placed on the bare glass to adhere to another ITO (or metal) substrate and the substrates firmly pressed together to desired separation. (c) Organic powder placed at the opening and capillary-filled into the cell by heating to its melting point. (d) Cell cooled to room temperature and electrical contact to ITO made.

coating. For example, optical anisotropy, induced by asymmetry in organic molecules and an important feature of some OMCs, is not experimentally detectable with samples where the molecules are randomly oriented (e.g., solutions, amorphous materials, polycrystalline films). Partially aligned systems, in which one or a few molecular layers are attached to stretched polymers<sup>17</sup> or in which the material is dissolved in liquid crystals,<sup>18,19</sup> can be used, but they often show some background interference generated by the substrate or through host-guest interactions. Moreover, grain boundaries and structural defects in such systems can distort or even dominate the charge-transport processes, making it difficult to model transport in these materials. On the other hand, single crystals grown

sufficiently large to make electrical contact are almost always too thick for optical characterization, e.g., obtaining the absorption spectra in the UV-vis region, where very thin single-crystal slices are needed for light penetration. Furthermore, optical modulation of the single-crystal electrical properties is difficult to study with thick samples, since light cannot penetrate across the sample. Accurate electric characterization in the dark is also difficult because of the highly insulative nature of most OMCs.

Over the past several years we have been using a technique for cell fabrication that results in the growth of large (several square millimeters) areas of organic single-crystal thin films ( $\sim 1 \mu\text{m}$  thick) between two pieces of indium-tin oxide (ITO) coated glass that serve as trans-

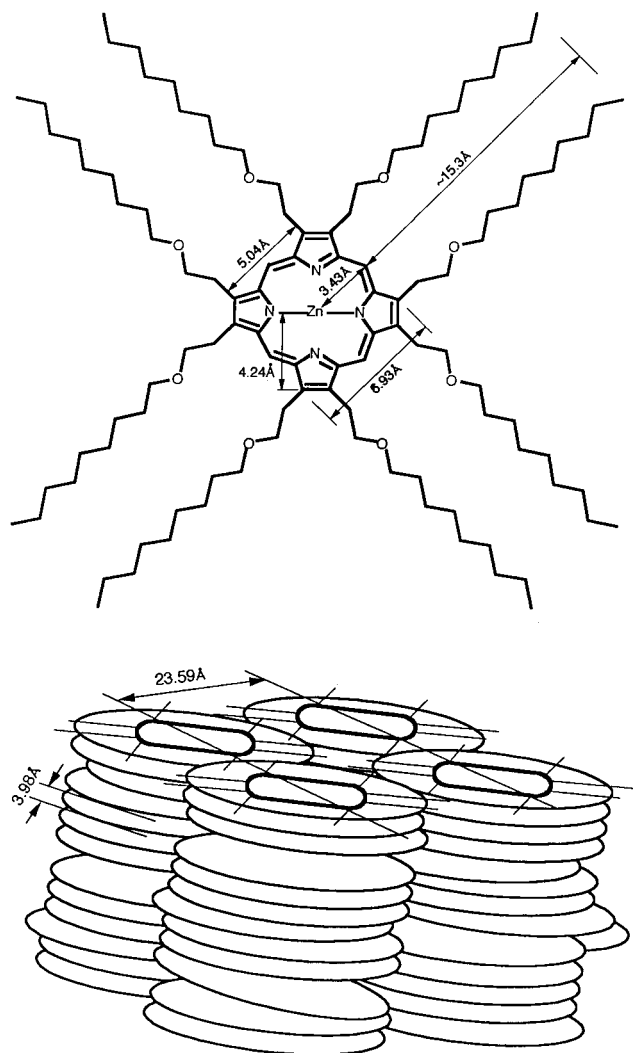
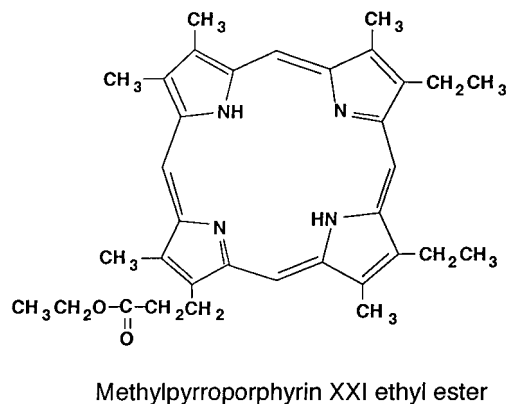


**FIGURE 2.** Chemical structure of ZnODEP (top) and schematic diagram of the crystal structure of ZnODEP showing crystal defects (bottom). Reprinted from ref 31. Copyright 1995 American Chemical Society.

parent electric contacts (Figure 1).<sup>14,20–22</sup> With these, many of the experimental difficulties with polycrystalline films and thick single crystals are largely eliminated. Optical and electrical characterizations can be carried out simultaneously at the same spot of a given crystal orientation, and as discussed below, information about how optical and electrical properties are affected by crystal structure can be obtained. The effects of the orientation of molecular columns, structural defects, and grain boundaries can be investigated for a number of OMCs.<sup>14,20,21</sup>

Of particular interest are OMCs that show a strong orientational dependence on electrical conductivity, sometimes called one-dimensional molecular solids.<sup>23–30</sup> An example of such a solid is zinc octakis( $\delta$ -decoxyethyl)porphyrin (ZnODEP) (Figure 2). Because of the effect of the long hydrocarbon chains attached to the porphyrin core, this material forms a discotic liquid crystal phase<sup>23,24,31</sup> in which the disk-shaped molecules are stacked regularly to form ordered molecular columns, each of which can be thought of as a molecular wire with higher conductivity along the column due to the better intermolecular  $\pi$ - $\pi$



Methylpyrroporphyrin XXI ethyl ester

**FIGURE 3.** Chemical structure of methylpyrroporphyrin XXI ethyl ester (top) and schematic diagram of porphyrin columnar structure with crystal defects (bottom). The  $x$ - $y$  plane is that of the ITO substrate, and the  $z$  axis is perpendicular to this plane. Reprinted from ref 20. Copyright 1996 American Chemical Society.

overlap than perpendicular to the columns.<sup>23,31</sup> These molecular columns remain fixed in the liquid crystal phase while the long tails remain somewhat flexible.<sup>31</sup> This phase solidifies to form a well-defined single-crystal solid on cooling. The nonpolar paraffin chains also serve as an insulating layer around each column (i.e., a wire coating) which spaces the columns apart and effectively hinders electronic communication between adjacent wires. We describe here several systems based on single-crystal thin films and their properties and possible applications.

### Effect of Crystal Structure and Molecular Column Orientation on Optical and Optoelectronic Properties

**Porphyrin.** Methylpyrroporphyrin XXI ethyl ester is a planar molecule that forms a columnar structure in the crystal as shown in Figure 3. Examination of porphyrin single-crystal thin films with visible light under magnification between two crossed polarizers provided clear evidence of the column orientation (Figure 4A).<sup>20</sup> Single-crystal domains with different orientation appear as different colors. For example, the two adjacent crystal domains shown on the right of Figure 4A(a) are barely distinguishable, but appear as two completely different colors under polarized light (Figure 4A(b,c)) due to bire-

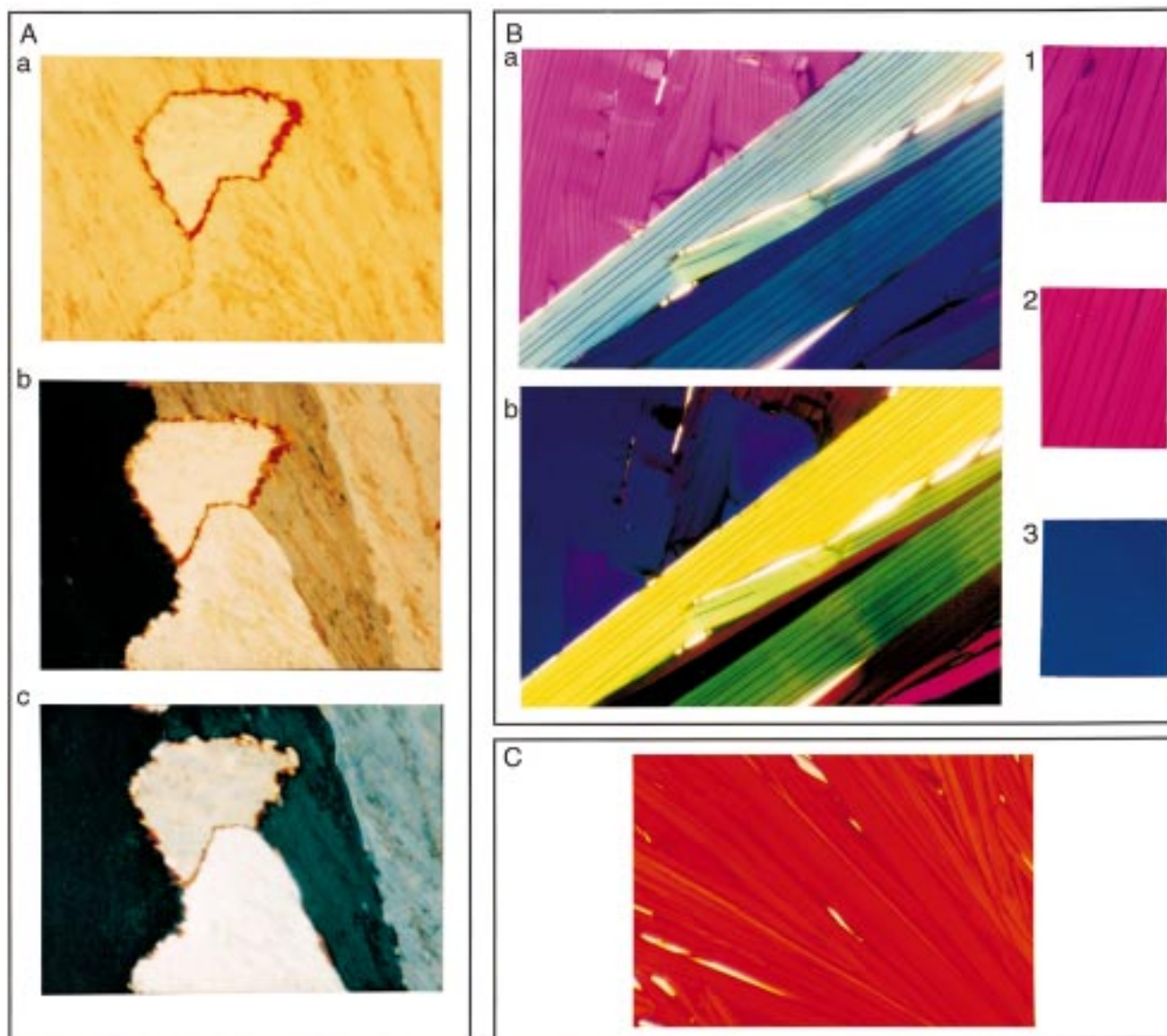


**FIGURE 4.** (A) Micrographs of methypyrroporphyrin XXI ethyl ester single crystals between two pieces of ITO-coated glass ( $\sim 2 \mu\text{m}$  thick; area of view,  $1 \text{ mm} \times 0.7 \text{ mm}$ ): (a) without polarizers, (b) between two crossed polarizers, and (c) after sample rotation from (b). The change in color with sample rotation allows recognition of crystal domains with slightly different orientations. Reprinted from ref 20. Copyright 1996 American Chemical Society. (B) Micrographs of SG3 single crystals between two pieces of ITO-coated glass ( $\sim 6 \mu\text{m}$  thick; area of view,  $1 \text{ mm} \times 0.67 \text{ mm}$ ) (a) without and (b) with polarizer. The direction of the polarized plane of light was rotated by (b)  $140^\circ$  clockwise from the vertical position. (c) The color of a purple spot (unpolarized light) with the polarizer at (1)  $60^\circ$ , (2)  $90^\circ$ , and (3)  $150^\circ$ . Reprinted from ref 14. Copyright 1997 American Chemical Society. (C) Micrograph of Sudan I single crystals between two pieces of ITO-coated glass ( $\sim 5 \mu\text{m}$  thick; area of view,  $470 \mu\text{m} \times 350 \mu\text{m}$ ). Reprinted from ref 21. Copyright 1997 American Chemical Society.

fringence effects.<sup>32,33</sup> Moreover, the color in each crystal domain changed with sample rotation between two crossed polarizers (Figure 4A(c)). As illustrated in Figure 3, if the  $x$ - $y$  plane is taken as the ITO surface,  $\phi$  represents the tilt angle of a porphyrin column relative to the  $z$  axis. At a given  $\phi$ , molecular columns still have all possible ( $360^\circ$ ) orientations within the  $x$ - $y$  plane. These different orientations are clearly distinguished with polarized light. When the sample was rotated, each crystal domain showed systematic changes in color, and the sequence of color changes was reproduced in other crystal domains. These domains, with apparently different orientations in the  $x$ - $y$  plane, have the same orientation relative to the  $z$  axis, in which case each crystal domain shows the same

sequence of colors upon rotation. Crystal domains showing a different sequence of color change with sample rotation have different orientations with respect to the  $z$  axis. The red color seen in a portion of the grain boundary in the center of Figure 4A did not change upon sample rotation with fixed polarizers, indicating an amorphous structure in this region, perhaps because it contains impurities that accumulated at the boundary during crystal growth.

The optoelectronic properties also strongly depend on crystal orientation. For example, in ZnOEDP the conductivity was much higher along porphyrin molecular columns than perpendicular to them because of better  $\pi$ - $\pi$  overlap. If the  $x$ - $y$  plane were parallel to the ITO surface

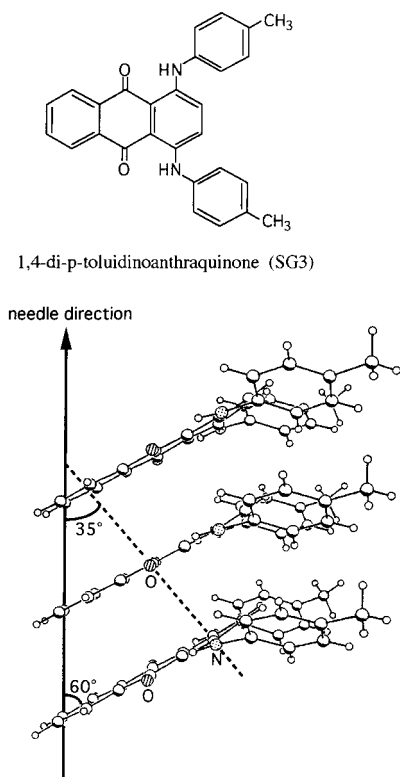


**FIGURE 5.** Chemical structure of SG3 (top) and crystalline packing structure of SG3 (bottom) viewed parallel to the *b* axis (the *b* axis is perpendicular to the plane of the paper). Reprinted from ref 14. Copyright 1997 American Chemical Society.

in Figure 3, then  $\phi = 0^\circ$  would represent the orientation with the highest conductivity between the ITO surfaces, while  $\phi = 90^\circ$  would yield the lowest conductivity. Between these two extremes there are many possible crystal orientations showing intermediate conductivity. Indeed, the photocurrents generated within different crystal domains (identified by polarized light microscopy) varied dramatically, i.e., by up to about an order of magnitude. When a light beam was scanned over a number of adjacent domains with different crystal orientation, the short-circuit photocurrent,  $I_{sc}$ , produced at different spots within the same crystal domain was essentially equal but showed sharp changes at the domain boundaries. These experiments provide direct evidence for the effect of the orientation of the molecular columns on the optoelectric properties. The photocurrents produced from those crystal domains with the same  $\phi$ , oriented differently only with respect to the *x*-*y* plane as distinguished by microscopy with crossed polarizers, were about the same, so the crystal orientation relative to the *z* axis was the determining factor in photocurrent generation.

**Solvent Green 3.** 1,4-Di-*p*-toluidinoanthraquinone (SG3) is a molecule characterized by the planes of the two phenyl groups out of the plane of the anthraquinone skeleton. In the crystal, the phenyl groups produce steric hindrance so that the SG3 molecules are slip-stacked to form regular molecular columns (Figure 5). Under a microscope, the ITO/SG3/ITO cells reveal a number of needle-shaped crystals with different colors which change

under polarized light (Figure 4B). The parallel straight lines shown on each domain are slip lines,<sup>14,20</sup> which are useful indicators of the crystal orientation. A domain showing only straight lines (oriented in one direction) is a true single-crystal domain with a fixed orientation; the color of that domain changes upon sample rotation between two crossed polarizers, and the color is always the same at any position within that domain. The domain showing a yellow color in Figure 4B(b) is such an example. In other cases the slip lines are curved or bent to some extent at some points as can be seen in the purple region in the upper-left corner of Figure 4B(a) which shows a purple color. In this corner, each different direction of the slip lines represents a particular crystal orientation that is clearly distinguishable with polarized light as different colors (Figure 4B(b)).

The three basic colors corresponding to three nearly orthogonal transition dipole moments in the crystal are blue, yellow-green, and purple.<sup>14</sup> The blue and yellow-green colors are transitions along the long and short axes of the anthraquinone skeleton, respectively, and the purple color is an intermolecular interaction between neighboring molecules. When a crystal needle is oriented so that only one of the three dipole moments is nearly parallel to the direction of the polarized light, the corresponding color dominates, while the other two colors are almost absent. Otherwise, a combination of the three basic colors appears. Since there are many possible orientations of the crystal needles, many different colors are observed in the thin films depending on which of the basic colors makes the largest contribution.<sup>14</sup> This can be confirmed by inspection of individual SG3 single-crystal needles grown from solution. In this case, the color of the crystals changes upon needle rotation. Such controllable color production might prove useful in optical applications.

The photocurrent also depends on crystal orientation. The  $I_{sc}$  was significantly larger in domains that showed a purple color than in those of the other colors under identical conditions, because light absorption in purple-colored domains occurs by an intermolecular electron transfer that is much more efficient in free charge carrier generation. In the other colored domains, only intramolecular electron transfer occurred initially upon irradiation and more of the excited states decayed to the ground states, leading to a lower photocurrent. As shown in Figure 6, the behavior of the  $I_{sc}$  as a function of time was also different in the crystal domains that produced the smallest photocurrents. In addition to the large difference in  $I_{sc}$ , an initial negative transient spike was seen in curve b of Figure 6, indicating a trapping/detrapping process.<sup>14</sup> When charge carriers hop along an unfavorable direction in a crystal, the possibility of being trapped is higher. These results suggest that the orientation of the purple crystals is much better for charge carrier transport than that of the other crystals. Indeed, the directions for observing colors other than purple are perpendicular to the molecular columns,<sup>14</sup> and the hopping of charge carriers between the columns is inherently slower than hopping along a column.

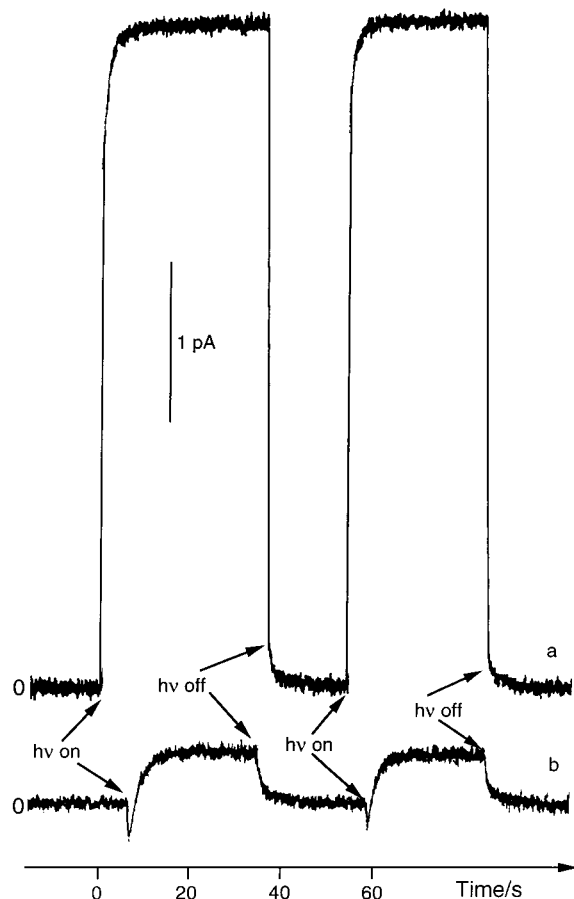


**FIGURE 6.** Short-circuit photocurrent, as a function of time, generated in crystal domains that were (a) purple and (b) blue in color. Of 16 separate domains sampled, the 5 smallest photocurrents were generated from green-blue- or blue-colored domains. The  $I_{sc}$  vs  $t$  curves for these 5 domains had the same shape as curve b while the other 11 domains generated curves similar to curve a. Reprinted from ref 14. Copyright 1997 American Chemical Society.

### Effect of an Electric Field on the Crystal Growth and Optoelectronic Properties

**Sudan I.** 1-(Phenylazo)-2-naphthol (Sudan I) is a planar molecule and forms molecular columns (Figure 7), leading to a needle-shaped crystal (Figure 4C). The resistivities perpendicular ( $\rho_{\perp}$ ) and parallel ( $\rho_{\parallel}$ ) to the needles are  $10^{16}$  and  $10^{14}$   $\Omega$  cm, respectively.<sup>21</sup> Better  $\pi$ - $\pi$  overlap enhances the electron hopping along the molecular columns.

When a bias voltage was applied between the two ITO electrodes during crystal growth of Sudan I, the resulting crystal was featureless and no needle structure was visible. The crystal needle axis, which was parallel to the ITO surface in field-free cells, tilts to some extent with respect to the ITO surface under an applied field, so that only the ends, rather than the whole length, of the needle crystals could be seen, similar to the electric field orientational effects in nonlinear optical applications.<sup>19,34</sup> Since,  $\rho_{\parallel} \ll \rho_{\perp}$ , any reorientation of the crystal needle with an electric field reduces the cell resistivity. This was confirmed by the measurement of the current in the dark and the photocurrent as a function of bias voltage. In both cases, the current vs voltage curves were straight lines, yielding

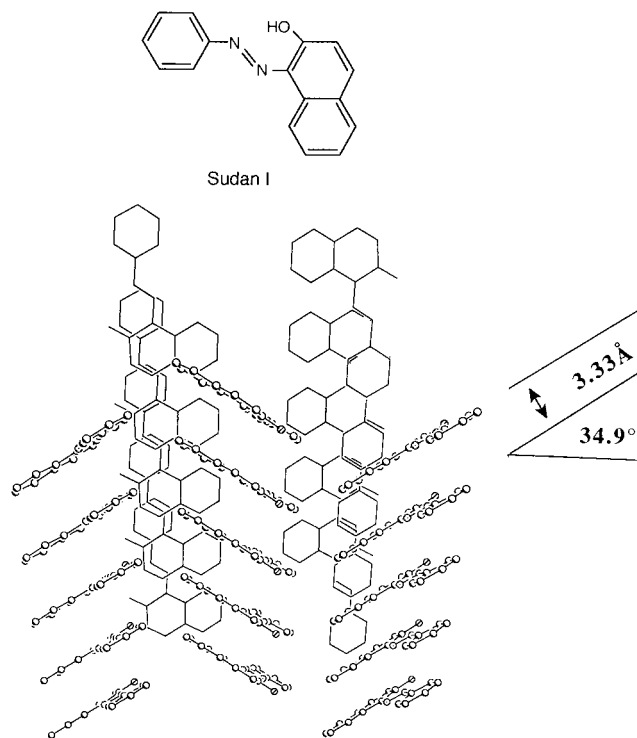


**FIGURE 7.** Chemical structure of Sudan I (top) and unit cell packing diagram for  $C_{16}H_{12}N_2O$  (bottom). The perpendicular distance between  $\pi$ -stacked molecules is shown. Reprinted from ref 21. Copyright 1997 American Chemical Society.

a measured conductance of a cell prepared with an electric field 8–9 times higher than in those prepared without a field. Moreover, the measured  $I_{sc}$  was increased about 14 times, indicating that the electric field-induced orientation of the Sudan I crystal needle not only increased the conductivity of the cell but also substantially improved the interfacial charge separation. This effect may be of use in the fabrication of organic optoelectronic devices.

**ZnODEP.** Cells of ITO/ZnODEP/ITO yielded short-circuit apparent quantum efficiencies,  $\Phi$  (electrons measured in external circuit/incident photons), of 0.5–0.7% for photocurrent production. When a field of 2000 V/cm was applied between the two ITO electrodes during melt crystallization in the cell preparation,  $\Phi$  increased more than 10 times,<sup>35</sup> while no morphology difference was observed between cells prepared with and without an electric field. In this case, since the molecular stacks are oriented perpendicular to the ITO surface, even without an electric field, the observed effect cannot be ascribed to crystal orientation. Rather the electric field effect is attributed to charge displacement in the film. Impurity ions could be displaced within the organic layer in the presence of the applied bias and cause a buildup of an internal electric field which would increase the probability of light-induced charge separation and movement. Dipole impurity molecules could also form an internal electric field after poling. The direction of  $I_{sc}$  was determined by the polarity of the bias voltage applied to the ITO/ZnODEP/ITO cell during preparation, suggesting the existence of an internal electric field or internal polarization. Indeed, the observed effect is similar to those in

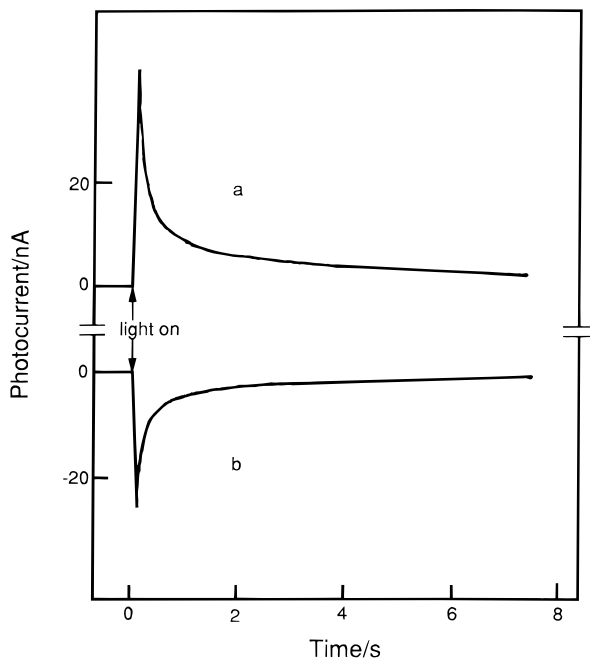


**FIGURE 8.** Short-circuit photocurrent of an ITO/ZnODEP/ITO cell as a function of time with a constant irradiation of 550 nm light after the cell had been subjected to irradiation with a 550 nm light beam under a bias of (a)  $-2$  and (b)  $+2$  V for 5 s followed by a rest period of 10 s under short-circuit conditions in the dark. Reprinted from ref 9. Copyright 1997 American Chemical Society.

which an electric field is applied to polymers at high temperature to generate electrets<sup>36</sup> or to produce persistent internal polarization.<sup>37,38</sup> The apparent buildup of an electric field by poling may be useful in the design of optoelectronic devices based on organic materials.

### Charge Trapping and Detrapping for Data Storage

Irradiation of ITO/ZnODEP/ITO cells under a bias (where the sign indicates the potential applied to the irradiated window with respect to the back contact) leads to a photocurrent and trapping of charge.<sup>6-10</sup> The  $I_{sc}$  spike seen under short-circuit irradiation with an ITO/ZnODEP/ITO cell previously exposed to irradiation under a bias represents detrapping of charge (Figure 8). The magnitude and the direction of the  $I_{sc}$  spike (i.e., anodic or cathodic) is determined by the magnitude and the sign of the bias voltage applied to the cells during the previous irradiation. The evolution of the  $I_{sc}$  spike from anodic to cathodic as a function of bias is shown in Figure 9. The curves in Figure 9 were obtained with the same sample under identical discharge conditions after the cell had been short-circuited for 10 s in the dark (to remove any residual charge on the ITO surfaces). The anodic discharge current spike decreases from curve a to curve b. A cathodic spike begins to appear in curve c and increases significantly in curves d and e. In general, under the same irradiation, a higher bias voltage during charging produced more stored charge. An important distinction in comparing this cell to a conventional capacitor is that irradiation is always needed for both the charge and discharge processes in

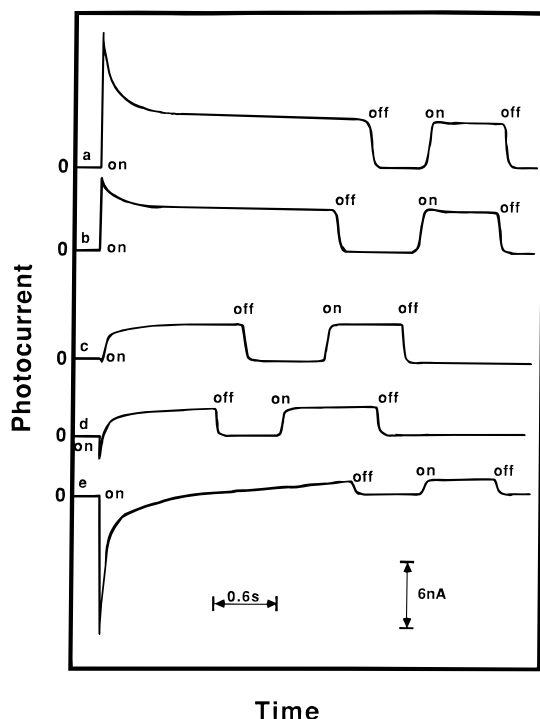


**FIGURE 9.** Photocurrent of an ITO/ZnODEP/ITO cell as a function of irradiation (550 nm) time under short-circuit conditions after irradiation of the cell with a 550 nm light under a bias of (a)  $-0.2$ , (b)  $-0.05$ , (c)  $+0.2$ , (d)  $+0.4$ , and (e)  $+1.2$  V for 5 s and a rest period of 10 s in the dark under short-circuit conditions. On and off indicate the irradiation is turned on and off. Reprinted from ref 9. Copyright 1997 American Chemical Society.

ITO/ZnODEP/ITO cells. This clearly indicates that charges are stored within the photoconductive insulator of the ZnODEP layer rather than on the two ITO surfaces, and therefore, no discharge occurs under short-circuit conditions in the dark. Trapping of charge probably occurs at crystal defects, grain boundaries, and chemical impurities within the ZnODEP layer.<sup>9</sup> The cell can store charge for a long time and be subjected to trapping and detrapping over 1.5 billion times without deterioration.<sup>9</sup> Moreover, trapping or detrapping could be carried out with a single 10 ns laser pulse (Figure 10) and the individual trapping sites could be as small as 40 nm in diameter,<sup>9</sup> corresponding to a density of  $\sim 8 \times 10^{10}/\text{cm}^2$ , making the system interesting for high-density information storage in the form of charge.

The material also appears adaptable to Si technology as demonstrated with the hybrid ITO/porphyrin/SiO<sub>2</sub>/Si structure.<sup>8</sup> With the addition of a thin insulator layer of SiO<sub>2</sub>, thinner storage films could be used with essentially total elimination of the steady-state photocurrents. By the application of an electric field, charges stored only at the outermost interfaces in the dark can accumulate at the SiO<sub>2</sub> surfaces under irradiation (Figure 11). Thus, a thousand times more charge could be stored with light (as compared with dark charge) as shown in Figure 12. This device can be considered as a light-controlled capacitor (Figure 13). This hybrid organic/Si structure has great advantages over conventional devices such as non-volatile semiconductor memories, for example, a floating

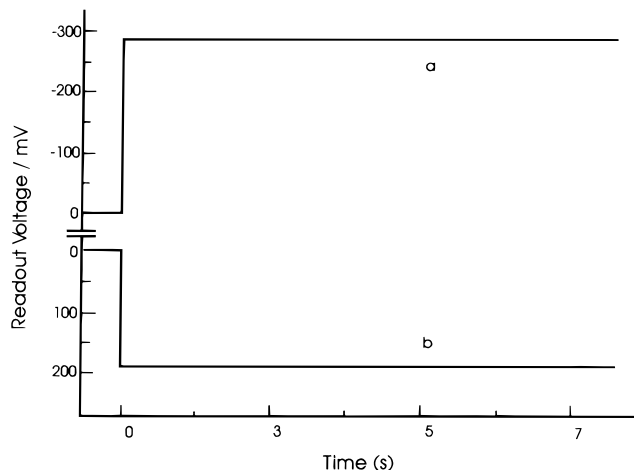


**FIGURE 10.** Readout voltage as a function of time. The data were stored by a single 10 ns laser pulse irradiation under potentials of (a)  $-1.0$  and (b)  $+1.0$  V. Reprinted from ref 9. Copyright 1997 American Chemical Society.

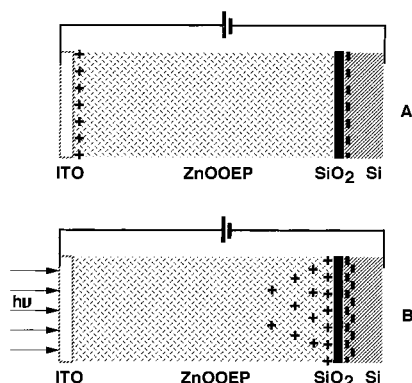


**FIGURE 11.** Schematic diagram of the operational principles for charge storage in a photoconductive medium (A) in the dark and (B) with irradiation. Reprinted with permission from ref 8. Copyright 1996 The Electrochemical Society.

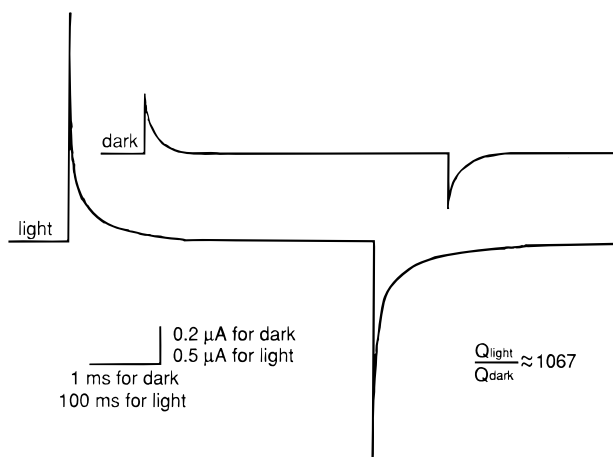


**FIGURE 12.** Charge and discharge characteristics of the cell with and without irradiation. A continuous square-wave potential ( $-0.4$  to  $+0.4$  V) was applied. Reprinted with permission from ref 8. Copyright 1996 The Electrochemical Society.

gate device (metal/ $\text{Si}_3\text{N}_4/\text{SiO}_2/\text{Si}$ ), where charges are forced by a high-voltage pulse to penetrate through the  $\text{SiO}_2$  layer (i.e., avalanche injection) and are stored in the  $\text{Si}_3\text{N}_4$  film for writing and can be removed with another

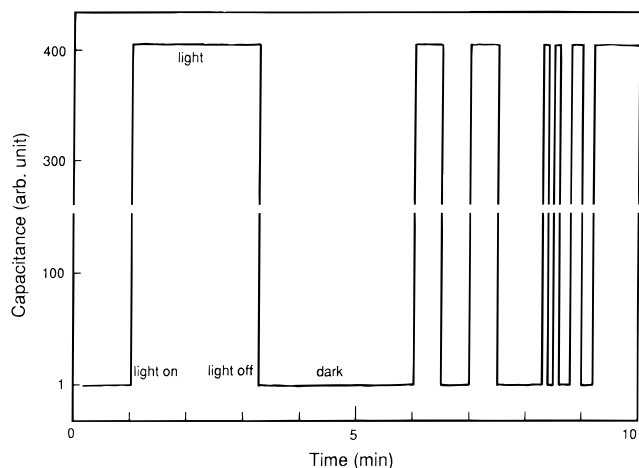


**FIGURE 13.** Response of the ITO/ZnOOEP/ $\text{SiO}_2/\text{Si}$  cell to irradiation as a function of time. A continuous sine-wave potential ( $-0.5$  to  $+0.5$  V) was applied. Reprinted with permission from ref 8. Copyright 1996 The Electrochemical Society.

pulse of opposite sign for erasing.<sup>39</sup> Such devices suffer inherently from high-voltage-induced degradation of the insulator layer which severely limits the number of write/erase cycles.<sup>40</sup> This problem does not exist in ITO/dye/ $\text{SiO}_2/\text{Si}$  cells where photoinduced charge and discharge occur under a low bias and no tunneling current through the insulator layer is required in its operation.<sup>8</sup>

### Characterization with an STM Tip

The characterization of thin OMC films by a scanning tunneling microscopic (STM) arrangement is also useful. The characteristics of large-area ITO/dye/ITO sandwich cells, especially for thin films less than  $1 \mu\text{m}$  thick, obtained by measurements between the ITO contacts can be critically dependent on a single impurity site, dust particle, or structural defect, leading to an isolated electric short. This makes the fabrication of useful thin-film cells challenging. This characterization problem can be overcome by replacing one ITO contact with an STM tip that addresses only a tiny area of the film. This configuration also allows the tip to be moved to sample many different sites on the same thin film. Moreover, the uniformity of film thickness is of less concern with this approach, since the tip can penetrate into the film to get thickness-dependent characteristics, as shown in Figure 14.

A typical current vs voltage plot from a Sudan I film, shown in Figure 15, indicates a high dark resistivity and good photoconductivity, desirable properties for electro-optical memory. Indeed, charges could be trapped within films upon irradiation under a proper bias and could be later released by the irradiation of the sample, producing a photodischarge current as shown in Figure 16. The  $I_{sc}$  spike was seen only with the very first irradiation and was not observed with subsequent irradiation (Figure 16b) unless the sample was recharged again after a steady state was reached. Figure 17 shows a series of photodischarge currents as a function of time from a Sudan I film which was previously charged under a different bias with the same level of irradiation. All of these charge/discharge

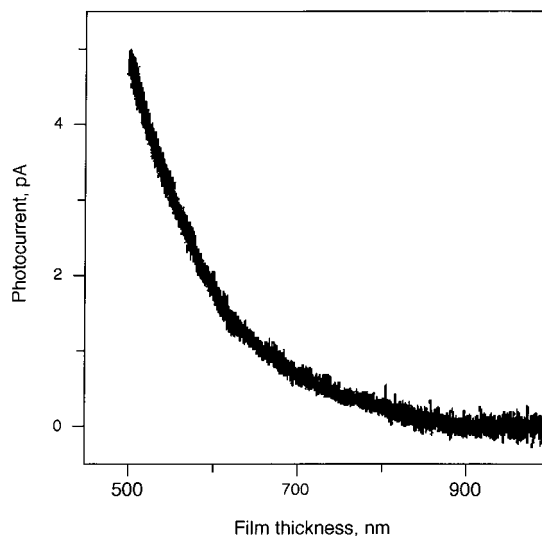


**FIGURE 14.** Relationship between the thickness of the Sudan I film and photocurrent under a bias of 5 V with tip positive. A sharp tip was moved through the layer (total film thickness  $\sim 1 \mu\text{m}$ ) at a rate of 5 nm/s. Reprinted from ref 10. Copyright 1998 American Chemical Society.

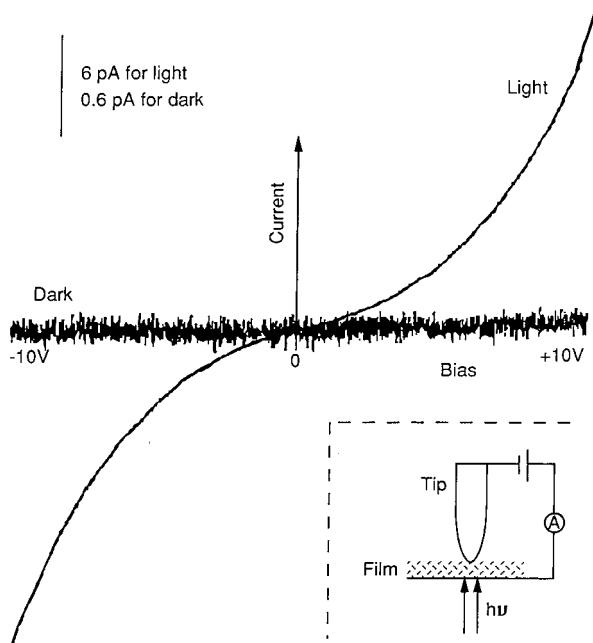


**FIGURE 15.** Current–voltage characteristics of a Sudan I thin film with a blunt tip contacting the film surface. Scan rate 0.2 V/s. The inset shows schematically the experimental setup. Reprinted from ref 10. Copyright 1998 American Chemical Society.

results were confirmed with large-area cells of ITO/Sudan I/ITO, indicating that the charge trapping/detrapping processes observed are independent of the physical size of the contact electrode and depend on the intrinsic properties of the Sudan I molecular crystal. Similar results from the same types of measurements were found with other dye molecules, including porphyrins, Disperse Red I, and Methyl Red.<sup>9,10</sup>

The STM tip was also used to estimate the spatial resolution of the charge trapping. As discussed in detail previously,<sup>9</sup> the sample was initially charged at one point and then the tip was moved to nearby sites to determine

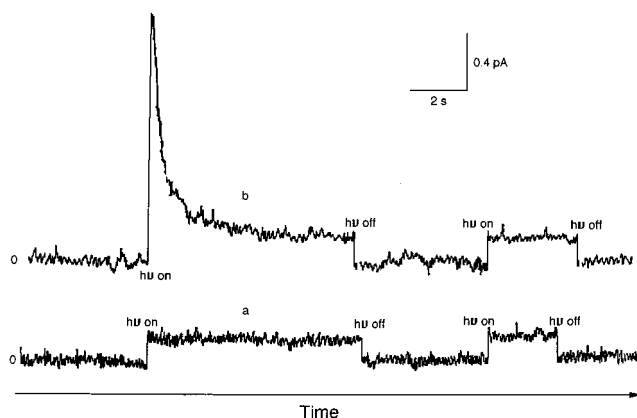


**FIGURE 16.** Short-circuit photocurrent as a function of time for Sudan I thin films where the sample (a) was not charged previously and (b) was previously photocharged under a bias of  $-10 \text{ V}$ . Reprinted from ref 10. Copyright 1998 American Chemical Society.

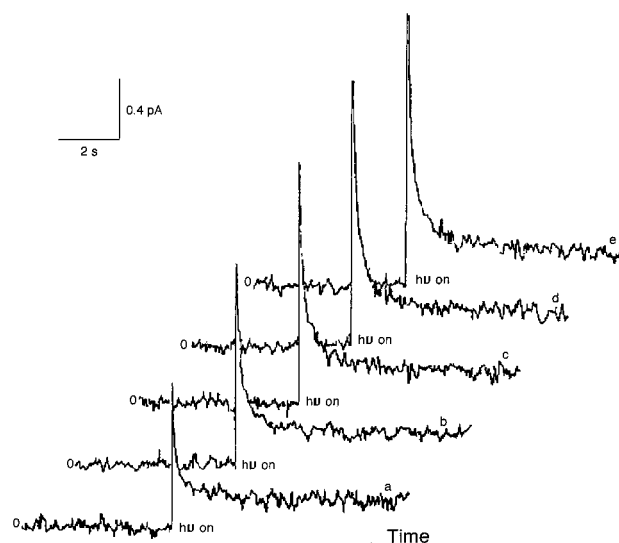


**FIGURE 17.** Photodischarge current as a function of time with Sudan I under short-circuit conditions. Charges were previously stored under potentials of (a) 2, (b) 4, (c) 6, (d) 8, and (e) 10 V. Reprinted from ref 10. Copyright 1998 American Chemical Society.

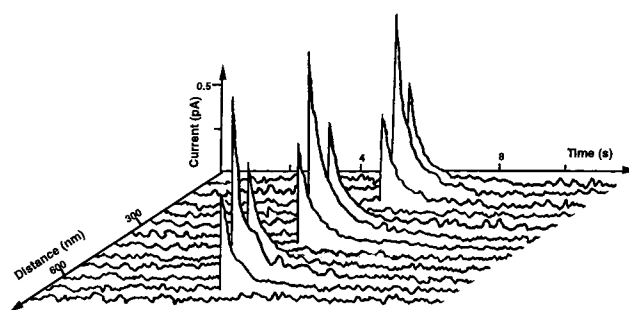


**FIGURE 18.** Discharge current as a function of time and position. Charges were stored under a bias of 10 V. Reprinted from ref 9. Copyright 1997 American Chemical Society.

the spatial distribution of trapped charge and the critical distance beyond which no discharge current was obtainable. This yields an estimate of the maximum size of an individual memory element and thus the data storage density under the given bias conditions.<sup>9</sup> Figure 18 shows a plot of discharge current as a function of time and

distance for three adjacent pixels within a ZnODEP film. Each pixel (charge storage site) was totally independent across a distance of less than 750 nm (for a 10 V bias). Since the ZnODEP is a bundle of insulated molecular wires (Figure 2), in principle an individual pixel could be as small as a single molecular column.

## Concluding Remarks

The weak intermolecular interactions in most OMCs offer interesting opportunities in the designed assemblage of tailored molecules into structures with desired properties. In the rich and diverse world of organics, we feel that the unique properties of individual molecules in the solid phase can best be characterized with single-crystal thin films. The larger intermolecular spacing may also allow the OMCs to be intercalated or doped with guest molecules to manipulate further their optical and electronic properties. An important direction is to investigate how guest molecules (dopants) affect the host molecular arrangement in the crystal and the optoelectronic properties.

## References

- (1) Sheats, J. R.; Antoniadis, H.; Hueschen, M.; Leonard, W.; Miller, J.; Moon, R.; Roitman, D.; Stocking, A. Organic Electroluminescent Devices. *Science* **1996**, *273*, 884.
- (2) *Organic Molecular Solids, Properties and Applications*; Jones, W., Ed.; CRC Press: Boca Raton, 1997.
- (3) Forrest, S. R. Ultrathin Organic Films Grown by Organic Molecular Beam Deposition and Related Techniques. *Chem. Rev.* **1997**, *97*, 1793.
- (4) *Molecular Electronics*; Ashwell, G. J., Ed.; Research Studies Press: Taunton, 1992.
- (5) Gregory, P. *High-Technology Applications of Organic Colorants*; Plenum Press: New York, 1991.
- (6) Liu, C.-Y.; Pan, H.-L.; Fox, M. A.; Bard, A. J. High-Density Nanosecond Charge Trapping in Thin Films of the Photoconductor ZnODEP. *Science* **1993**, *261*, 897.
- (7) Liu, C.-Y.; Pan, H.-L.; Bard, A. J.; Fox, M. A. Optoelectric Memories with Photoconductive Thin Films. U.S. Patent 5 327 373.
- (8) Liu, C.-Y.; Hasty, T.; Bard, A. J. Electrooptical Charge Trapping in Zinc Porphyrin Films on Indium Tin Oxide and  $\text{SiO}_2/\text{Si}$ . *J. Electrochem. Soc.* **1996**, *143*, 1916.
- (9) Liu, C.-Y.; Pan, H.-L.; Fox, M. A.; Bard, A. J. Reversible Charge Trapping/Detrapping in a Photoconductive Insulator of Liquid Crystal Zinc Porphyrin. *Chem. Mater.* **1997**, *9*, 1422.
- (10) Liu, C.-Y.; Bard, A. J. Optoelectric Charge Trapping/Detrapping in Thin Solid Films of Organic Azodyes—Application of Scanning Tunneling Microscopic Tip Contact to Photoconductive Films for Data Storage. *Chem. Mater.* **1998**, *10*, 840.
- (11) Silinsh, E. A.; Capek, V. *Organic Molecular Crystals: Interaction, Localization, and Transport Phenomena*; American Institute of Physics: New York, 1994.
- (12) Pope, M.; Swenberg, C. E. *Electronic Processes in Organic Crystals*; Clarendon Press: Oxford, 1982.
- (13) Broude, V. L.; Rashba, E. I.; Sheka, E. F. *Spectroscopy of Molecular Excitons*; Springer-Verlag: Berlin, 1985.
- (14) Saito, T.; Liu, C.-Y.; Bard, A. J. Orientational Dependence of the Color and Photoconductivity of 1,4-Di-p-toluidino-anthraquinone Single Crystals. *Chem. Mater.* **1997**, *9*, 1318.
- (15) Kao, K. C.; Hwang, W. *Electrical Transport in Solids*; Pergamon Press: Oxford, 1981.
- (16) Wright, J. D. *Molecular Crystals*; Cambridge University Press: Cambridge, 1987.
- (17) Thulstrup, E. W.; Michl, J. *Elementary Polarization Spectroscopy*; VCH: New York, 1989; pp 27–49.
- (18) Castellano, J. A. *Handbook of Display Technology*; Academic Press: San Diego, 1992.
- (19) Williams, D. J. Organic Polymeric and Non-Polymeric Materials with Large Optical Nonlinearities. *Angew. Chem., Int. Ed. Engl.* **1984**, *23*, 690.
- (20) Liu, C.-Y.; Tang, H.; Bard, A. J. Effect of Orientation of Porphyrin Single-Crystal Slices on Optoelectronic Properties. *J. Phys. Chem.* **1996**, *100*, 3587.
- (21) Liu, C.-Y.; Lynch, V.; Bard, A. J. Effect of an Electric Field on the Growth and Optoelectronic Properties of Quasi-One-Dimensional Organic Single Crystals of 1-(Phenylazo)-2-naphthol. *Chem. Mater.* **1997**, *9*, 943.
- (22) Gregg, B. A.; Fox, M. A.; Bard, A. J. Photovoltaic Effect in Symmetrical Cells of a Liquid Crystal Porphyrin. *J. Phys. Chem.* **1990**, *94*, 1586.
- (23) Fox, M. A.; Vincent, J. R.; Melamed, D.; Torimoto, T.; Liu, C.-Y.; Bard, A. J. Effect of Structure Variation on Photocurrent Efficiency in Alkyl-Substituted Porphyrin Solid-State Thin Layer Photocells. *Chem. Mater.* **1998**, *10*, 1771.
- (24) Gregg, B. A.; Fox, M. A.; Bard, A. J. 2,3,7,8,12,13,17,18-Octakis( $\beta$ -hydroxyethyl)porphyrin (Octaethanolporphyrin) and Its Liquid Crystalline Derivatives: Synthesis and Characterization. *J. Am. Chem. Soc.* **1989**, *111*, 3024.
- (25) Chandrasekhar, S.; Sadashiva, B. K.; Suresh, K. A. Liquid Crystals of Disk-Like Molecules. *Pramana* **1977**, *9*, 471.
- (26) Goodby, J. W.; Robinson, P. S.; Teo, B.-K.; Clad, P. E. The Discotic Phase of Uro-Porphyrin I Octa-n-Dodecyl Ester. *Mol. Cryst. Liq. Cryst. Lett.* **1980**, *56*, 303.
- (27) Morelli, G.; Ricciardi, G.; Roviello, A. Discotic Mesomorphism of the 2,3,7,8,12,13,17,18-Octakis-(Octylthio)Tetraazaporphyrin Copper(II) Complex. *Chem. Phys. Lett.* **1991**, *185*, 468.
- (28) Simon, J.; Bassoul, P. Phthalocyanine Based Liquid Crystals: Towards Submicronic Devices. In *Phthalocyanines, Properties and Applications*; Leznoff, C. C., Lever, A. B. P., Eds.; VCH: New York, 1989; Vol. 2, p 223 and references therein.
- (29) Boden, N.; Bushby, R. J.; Clements, J. Mechanism of Quasi-One-Dimensional Electronic Conductivity in Discotic Liquid Crystals. *J. Chem. Phys.* **1993**, *98*, 5920.
- (30) Boden, N.; Borner, R. C.; Bushby, R. J.; Clements, J. First Observation of an n-Doped Quasi-One-Dimensional Electronically-Conducting Discotic Liquid Crystal. *J. Am. Chem. Soc.* **1994**, *116*, 10807.
- (31) Liu, C.-Y.; Pan, H.-L.; Tang, H.; Fox, M. A.; Bard, A. J. Effect of Structural Order on the Dark and Photocurrents in Zinc Octakis (b-decoxyethyl)porphyrin Thin-Layer Cells. *J. Phys. Chem.* **1995**, *99*, 7632.
- (32) Pankove, J. I. *Optical Processes in Semiconductors*; Dover: New York, 1975.

- (33) Bousfield, B. *Surface Preparation and Microscopy of Materials*; John Wiley & Sons: New York, 1992.
- (34) *Nonlinear Optical Properties of Organic Molecules and Crystals*; Chemla, D. S., Zyss, J., Eds.; Academic Press: Orlando, FL, 1987; Vol. 1.
- (35) Liu, C.-Y.; Bard, A. J. Enhanced Quantum Efficiencies and Short-circuit Photocurrents in Solid Porphyrin Thin Film Cells by Internal Electric Fields. *J. Am. Chem. Soc.* **1998**, *120*, 5575.
- (36) Sessler, G. M. *Electrets*; Springer-Verlag: Berlin, 1987.
- (37) Freeman, J. R.; Kallmann, H. P.; Silver, M. Persistent Internal Polarization. *Rev. Mod. Phys.* **1961**, *33*, 553.
- (38) Kallmann, H. P.; Rosenberg, B. Persistent Internal Polarization. *Phys. Rev.* **1955**, *97*, 1596.
- (39) Sze, S. M. *Physics of Semiconductor Devices*, 2nd ed.; John Wiley & Sons: New York, 1981.
- (40) Prince, B. *Semiconductor Memories*, 2nd ed.; John Wiley & Sons: New York, 1991.

AR980031N